Mohammed Rabius Sunny[1]
Department of Aerospace and Ocean Engineering,
Virginia Polytechnic Institute and State University,
Blacksburg, VA 24061
e-mail: sunny@vt.edu

Rakesh K. Kapania
Mitchell Professor of Aerospace and Ocean Engineering,
Virginia Polytechnic Institute and State University,
Blacksburg, VA 24061
e-mail: rkapania@vt.edu

Ronald D. Moffitt
Institute for Advanced Learning and Research,
Danville, VA 24540
e-mail: rmoffitt@vt.edu

Amitabh Mishra
Department of Computer Science,
Johns Hopkins University,
Baltimore, MD 21218
e-mail: amitabh@cs.jhu.edu

Nakhiah Goulbourne
Department of Mechanical Engineering,
Virginia Polytechnic Institute and State University,
Blacksburg, VA 24061
e-mail: nakg@vt.edu

A Modified Fractional Calculus Approach to Model Hysteresis

This paper describes the development of a fractional calculus approach to model the hysteretic behavior shown by the variation in electrical resistances with strain in conductive polymers. Experiments have been carried out on a conductive polymer nanocomposite sample to study its resistance-strain variation under strain varying with time in a triangular manner. A combined fractional derivative and integer order integral model and a fractional integral model (with two submodels) have been developed to simulate this behavior. The efficiency of these models has been discussed by comparing the results, obtained using these models, with the experimental data. It has been shown that by using only a few parameters, the hysteretic behavior of such materials can be modeled using the fractional calculus with some modifications. [DOI: 10.1115/1.4000413]

1 Introduction

Hysteresis represents a property of systems that show dependence on the input history applied to it, i.e., the output at any time instant depends on the input applied to the system both at the present time as well as at the previous history; consequently the same instantaneous value of the input can give different outputs depending on the entire input history. Hysteretic phenomena are encountered in various branches of engineering, such as magnetic hysteresis, electrical hysteresis, ferroelectric hysteresis, electron beam hysteresis, adsorption hysteresis, and so on. The viscoelastic behavior of composite laminates [1,2] and the rheological behavior of polymers [3] are other well-known examples of hysteretic behavior.

Different mathematical models have been developed, depending on the type of hysteretic behavior, and successfully applied in these fields. Resistance-strain variation in conductive polymers is an important property that requires a proper hysteresis model for its characterization. Conductive polymers generally have a high electrical conductivity and a low elastic modulus. They can be used as possible sensors to measure large strains in inflatable structures, such as tires. Our research has been motivated by our need to use conductive polymers for large-strain sensing. Some studies on the unsteady behavior of conductive polymers can be found in Refs. [4–6]. Hysteresis models are either physics based or empirical. Physics based models, being mainly microscopic and semimicroscopic, involves the application of the energy principle and thermodynamic, electromagnetic, or other laws depending on type of the problem at the grain level [7]. The main disadvantage with such models is the requirement of a large number of material parameters.

Our goal was to develop a mathematical model for the calibration of a large-strain sensor, we were therefore more interested in empirical models that require fewer parameters and are suitable for practical applications, such as the structural health monitoring of inflatable structures. We first reviewed two of the several existing hysteresis models, namely, the Preisach and the fractional calculus approaches. We found out that both these approaches in their traditionally used forms did not lend their application to our data readily. We developed a modified fractional calculus approach to represent the path-dependent behavior of conductive polymers.

Preisach [8] in 1935 developed the well-known model to represent the path-dependent behavior of magnetic materials based on some plausible hypothesis concerning the physical mechanisms of magnetism. Everett and Whitton [9] independently developed the model for adsorption hysteresis. In the Preisach model, the hysteresis is considered as a combination of numbers of elementary hysteresis operators $\gamma_{\alpha,\beta}(u(t))$, which can be represented by rectangular loops with α and β as the up- and down-switching values, respectively, as shown in Fig. 1. When the input increases monotonically and reaches a value α, the operator goes to the upswitched state and reaches a value of 1; and when the input decreases monotonically and reaches a value β, the operator goes to the downswitched state and reaches a value of -1. The governing equation for the classical Preisach model is given in Eq. (1). Here the output $f(t)$ is assumed to be a weighted combi-

[1]Corresponding author.

Contributed by the Applied Mechanics Division of ASME for publication in the JOURNAL OF APPLIED MECHANICS. Manuscript received July 29, 2008; final manuscript received July 28, 2009; published online February 1, 2010. Assoc. Editor: Krishna Garikipati.

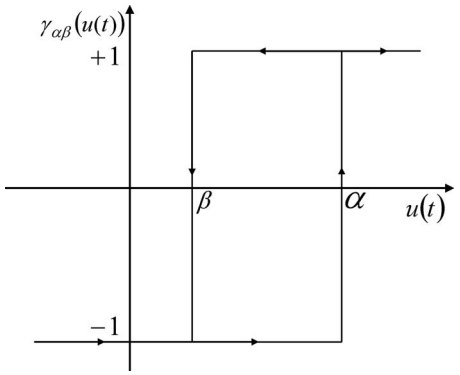

Fig. 1 Operator in the Preisach model

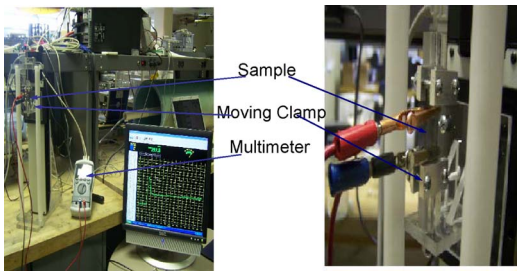

Fig. 2 Experimental setup

nation of the outputs of different elementary hysteretic operators; $\mu(\alpha,\beta)$ is the weight multiplied by the output of the operator $\gamma_{\alpha,\beta}(u(t))$ and the combination of $\mu(\alpha,\beta)\gamma_{\alpha,\beta}(u(t))$ for different α and β gives the output $f(t)$. The main aim is to determine the values of the weight function $\mu(\alpha,\beta)$ for different possible combinations of α and β to characterize the system

$$f(t) = \int \int_{\alpha>\beta} \mu(\alpha,\beta)\gamma_{\alpha,\beta}(u(t))d\alpha d\beta \tag{1}$$

Subsequently, several modifications were proposed to take care of the dependence of the output on the rate of input, the stabilization process, and so on. Cornejo and Missell [10] used the Preisach model to model nanocrystalline magnets. Roshko and Huo [11] characterized the irreversible response of a ferromagnet perovskite ($SrRuO_3$) with a Curie temperature of 160 K. Vandenbossche et al. [12] investigated the application of magnetic hysteresis measurement combined with the Preisach model for the evaluation of the fatigue damage progression. The determination of the weight function $\mu(\alpha,\beta)$ and a very high computation time are major problems in using the Preisach model. Schiffer and Ivanyi [13] showed the use of wavelets to solve these problems. The weight functions $\mu(\alpha,\beta)$ were derived for some (α,β) and two-dimensional wavelet average interpolation transform was applied to interpolate the function at other (α,β). Yu et al. [14] represented system outputs and the Preisach function by wavelet approximation.

Fractional derivatives were first discussed in 1695 by l'Hospital in a letter to Leibniz [15,16]. Later on researchers like Euler [17], Lacroix [18], Hardy [19], and Osler [20] made significant contributions to the theory of fractional calculus. This approach has proven to be very effective in modeling the dynamic behaviors of different kinds of materials, especially of viscoelastic materials showing hysteresis coupled with relaxation. Nutting [21] observed that stress relaxation could be modeled by fractional powers of time. This can be viewed as the progenitor of the fractional calculus approach of modeling viscoelastic behavior [22]. Gemant's [23] observation on stiffness and damping properties of viscoelastic materials to be proportional to the fractional powers of frequency was another motivating factor behind this. The basic principle behind this type of modeling is to express the relation of time-dependent output $f(t)$ with the time-dependent input $u(t)$ as an equation involving fractional differential and integral operators. An example of such an equation can be Eq. (2). D^a represents derivative and J^a represents integral of order a. Here $0<a<1$. $C_k, a_k (k=1,\ldots,N)$ are material parameters, which are determined by using experimental data

$$f(t) + \sum_{k=1}^{L} C_k D^{a_k}(f(t)) = C_{L+1}u(t) + \sum_{k=L+2}^{N} C_k D^{a_k}(u(t)) + \sum_{k=N+1}^{M} C_k J^{a_k}(u(t)) \tag{2}$$

Output $f(t)$ for time-dependent input $u(t)$ is determined experimentally and by minimizing the sum of the square of difference between the output obtained from the experiment and the output predicted by the model at the data points, the values of $C_k, a_k (k=1,\ldots,N)$ are determined. Depending on the value of N, numbers of unknown parameters vary in the model. Scott-Blair and Reiner [24], and Belavine et al. [25] applied fractional derivatives in the field of rheology and electrochemistry, respectively. Bagley and Torvik [26,27] showed the use of fractional derivatives to model the viscoelastic behavior. Thermodynamic constraints, based on a non-negative rate of energy dissipation and non-negative internal work were used for the selection of material parameters. de Espindola et al. [28] proposed a model based on four unknowns in the fractional differential equation to identify different mechanical properties of viscoelastic material. Horr and Schmidt [29] modeled frequency dependent damping characteristics of viscoelastic materials using fractional derivatives. Davis et al. [30] used a fractional derivative to determine constitutive properties of brain parenchyma. They used the fractional Zener model with four unknowns and obtained relaxation and creep properties of the material.

The main advantage of the fractional calculus model is that it needs a very few number of parameters for characterization. This has been successfully applied to model the variation in resistance with strain in the conductive polymer. First of all, experiments carried out on a conductive polymer to study the variation in resistance with strain in the material has been described. Then, behaviors of different functions operated by fractional calculus operators have been discussed and the application of these operators to simulate the behavior of the material has been shown. Two models based on the fractional calculus approach have been developed. Results of these models have been compared with the experimental result and concluding remarks have been made.

2 Experimental Details

The conductivity test was carried out on a conductive polymer sensor to study its variation in electrical resistance with strain. The experimental setup used for this test is shown in Fig. 2. The sample was clamped at the two ends of the linear stage (NLS4-10-25 by Newmark Systems Inc., Mission Viejo, CA). The top clamp of it is fixed. The bottom clamp can move and apply strain to the material at a desired rate. Movement of the bottom clamp can be controlled by the "IMS LYNX TERMINAL," a software provided by Intelligent Motion Systems Inc., Marlborough, CT. This helps us to apply strain to the material with a desired rate. The two ends of the sample close to the clamps are connected to a 46-range digital multimeter with an interface to a computer through a serial port (RS-232). The multimeter shows the resistance of the portion

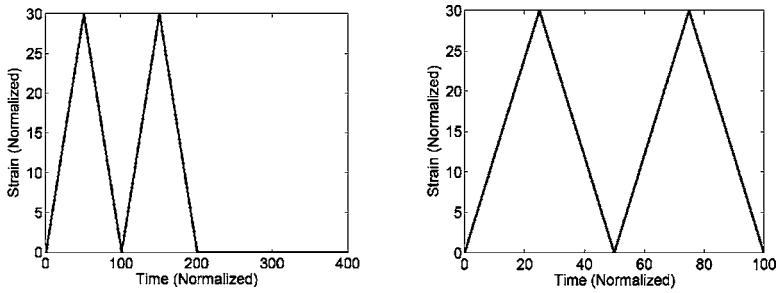

Fig. 3 Applied strain

of the material between the connected ends. Readings of the multimeter are stored in the computer through a program "METERVIEW 1.0," provided by Radioshack, Blacksburg, VA. Using this setup, a time-dependent strain can be applied to the sample and its resistance can be measured at different time instants at different strain levels. Time-dependent cyclic strain input, as shown in Fig. 3(*a*), with a strain rate of 3/20 percent per second was applied to the system and time-dependent resistance was measured. The change in output resistance with input strain and time is shown in Figs. 4(*a*) and 4(*b*). The output obtained from the experiment contained a high frequency noise, which was removed by using a low-pass filter to smooth the experimentally obtained curve. In Figs. 4(*a*) and 4(*b*) unfiltered and smoothed (filtered) data have been presented. Smoothed data obtained after performing two sets of experiments have been shown to ensure the repeatability of the experiment. Smoothed data obtained from the first experiment has been used later on for developing the mathematical model. Let us term this data set as data set 1. After this the material was allowed to relax and another experiment was performed by applying a strain, as shown in Fig. 3(*b*), with a higher strain rate of 3/10 percent per second. Results obtained from this experiment are shown in Fig. 4(*c*). Let us call it data set 2.

3 Fractional Calculus Operators and Their Properties

Fractional calculus allows the definition of the derivative and integral of generalized order. This often helps in creating a compact representation of a system. Fractional derivative D^a and fractional integral J^a of a function $u(t)$ can be defined as

$$D^a(u(t)) = \frac{1}{\Gamma(1-a)}\frac{d}{dt}\int_0^t \frac{u(\tau)}{(t-\tau)^a}d\tau \tag{3}$$

$$J^a(u(t)) = \frac{1}{\Gamma(1+a)}\frac{d}{dt}\int_0^t \frac{u(\tau)}{(t-\tau)^{-a}}d\tau \tag{4}$$

Here, Γ is the gamma function. Fractional derivatives and integrals at time t_m can be calculated numerically by using the following expressions [15,31]:

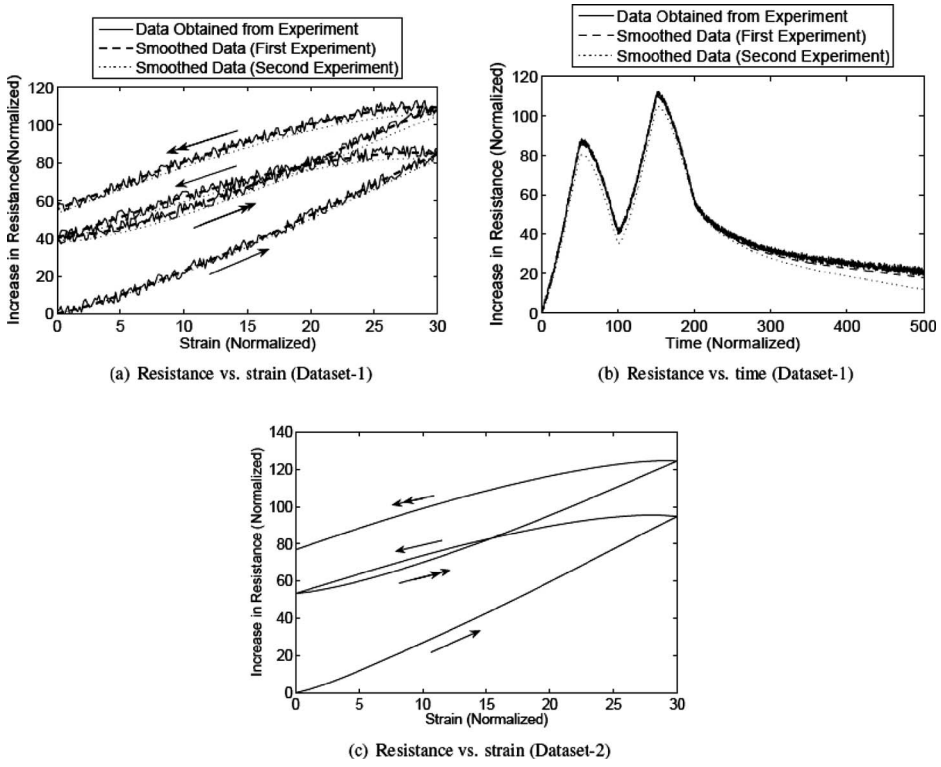

Fig. 4 Experimental results

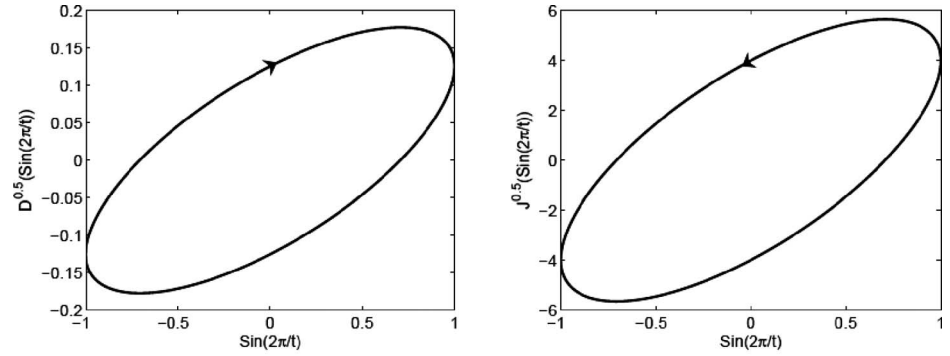

(a) $D^{0.5}(Sin(2\pi/t))$ vs. $Sin(2\pi/t)$ (b) $D^{0.5}(Sin(2\pi/t))$ vs. $Sin(2\pi/t)$

Fig. 5 Derivative and integral of order 0.5

$$D^a(u(t)) = \frac{\Delta t^{-a}}{\Gamma(2-a)}\left[\frac{(1-a)}{m^a}u_0 + \sum_{j=0}^{m-1}((j+1)^{(1-a)} - j^{(1-a)})(u_{m-j} - u_{m-j-1})\right] \tag{5}$$

$$J^a(u(t)) = \frac{\Delta t^{a}}{\Gamma(2+a)}\left[\frac{(1+a)}{m^{-a}}u_0 + \sum_{j=0}^{m-1}((j+1)^{(1+a)} - j^{(1+a)})(u_{m-j} - u_{m-j-1})\right] \tag{6}$$

where $u_j = u(j\Delta t)$. The time interval $[0, t_m]$ is divided into m equally spaced sections of size Δt.

In the frequency domain Fourier transform of $u(t)$ and its derivatives and integrals of order a are related by Eqs. (7) and (8)

$$G_D(\omega) = (i\omega)^a U(\omega) \tag{7}$$

$$G_J(\omega) = (i\omega)^{-a} U(\omega) \tag{8}$$

where $U(\omega)$, $G_D(\omega)$, and $G_J(\omega)$ denotes the Fourier transform of $u(t)$, its derivative and integral.

Derivatives and integrals of pure sinusoidal functions can be characterized by a phase-shift and the modulation of amplitude, depending on the frequency of the sinusoidal function and order of derivatives and integrals, as shown in the following equations:

$$D^a(\sin(\omega t)) = \omega^a \sin\left(\omega t + \frac{\pi a}{2}\right) + \frac{(\omega t)^{-1-a}}{\omega\Gamma(-a)} - \frac{(\omega t)^{-3-a}}{\omega^3\Gamma(-a-2)} + \ldots \tag{9}$$

$$D^a(\cos(\omega t)) = \omega^a \cos\left(\omega t + \frac{\pi a}{2}\right) + \frac{(\omega t)^{-2-a}}{\omega^2\Gamma(-a-1)} - \frac{(\omega t)^{-4-a}}{\omega^4\Gamma(-a-3)} + \ldots \tag{10}$$

$$J^a(\sin(\omega t)) = \omega^{-a} \sin\left(\omega t - \frac{\pi a}{2}\right) + \frac{(\omega t)^{-1+a}}{\omega\Gamma(a)} - \frac{(\omega t)^{-3+a}}{\omega^3\Gamma(a-2)} + \ldots \tag{11}$$

$$J^a(\cos(\omega t)) = \omega^{-a} \cos\left(\omega t - \frac{\pi a}{2}\right) + \frac{(\omega t)^{-2+a}}{\omega^2\Gamma(a-1)} - \frac{(\omega t)^{-4+a}}{\omega^4\Gamma(a-3)} + \ldots \tag{12}$$

The first term in both Eqs. (9) and (10) shows a forward phase-shifting of the periodic function being operated by the differential operator by an amount $\pi a/2$, where a is the order of the derivative. When the derivative of the periodic function is plotted against the actual periodic function it gives rise to a clockwise hysteresis loop due to this forward phase-shift, as shown in Fig. 5(*a*). Similarly, the first term in both Eqs. (11) and (12) show a backward phase-shifting of the periodic function being operated by the integral operator by an amount $\pi a/2$, where a is the order of the integral. When the integral of the periodic function is plotted against the actual periodic function it gives rise to a anticlockwise hysteresis loop due to this backward phase-shift, as shown in Fig. 5(*b*).

A constant function x_0 decays sharply while operated by fractional derivatives and increases with time at a decaying rate on being operated by fractional integrals, as shown in Eqs. (13) and (14)

$$D^a(x_0) = \frac{x_0 t^{-a}}{\Gamma(1-a)} \tag{13}$$

$$J^a(x_0) = \frac{x_0 t^{a}}{\Gamma(1+a)} \tag{14}$$

Hence, under the operation of a fractional differential operator the nonharmonic component of a function dies out shortly and its harmonic components gives rise to a closed loop clockwise hysteresis and on the other hand the same function shows an anticlockwise hysteresis with a hysteresis loop moving upward with a number of cycles when it is operated by a fractional integral operator.

4 Development of the Fractional Calculus Model

The main features of the hysteresis in the resistance-strain behavior of conductive polymer are the following:

1. The anticlockwise hysteresis loop moves upwards with a number of cycles and the width of the hysteresis loop does not necessarily remain constant.
2. When the strain is kept at a constant level the value of the resistance is observed to relax.

Based on these observations and the discussion in Sec. 3 two models are developed in this study to model these features. These models are based upon representing the output resistance as a combination of different fractional order derivatives and integrals with some modifications. In these models, an error function e_m has been defined

$$e_m = R_{ex}(t_m) - R(t_m) \tag{15}$$

$R_{ex}(t_m)$ is the value of the resistance obtained from the experiment at $t = t_m$ and $R(t_m)$ is the resistance obtained from the mathematical model. Then considering all the data points in the interval $[t_0, t_n]$, error e has been defined. Error e is minimized for all

the models to find the unknown parameters associated with these models. Error minimizations were accomplished using the function "fmincon" in the optimization toolbox of MATLAB

$$e = \sum_{m=0}^{n} (R_{ex}(t_m) - R(t_m))^2 \tag{16}$$

4.1 Model 1: Combined Fractional Derivative and Integer Order Integral Model. In this model the change in resistance has been assumed to be a combination of a linear function of strain, fractional order derivatives of strain, with each frequency component shifted backward and integer order integral of different powers of strain, multiplied by an exponentially decaying function. It can be written as

$$R(t) = C_0\varepsilon(t) + \sum_{k=1}^{N} C_k D_{Ph}^{a_k}(\varepsilon(t)) + \sum_{l=1}^{M-N} C_{l+M} \int_0^t e^{-p_l(t-\tau)} \varepsilon(\tau)^{q_l} d\tau \tag{17}$$

$D_{Ph}^{a_k}$ is a derivative of order a_k with a phase of the each frequency component of derivative shifted by $\pi b_k/2$, where $b_k < 0$. If $\varepsilon(t)$ can be written in terms of its Fourier components as

$$\varepsilon(t) = \sum_{i=0}^{N} x_i \cos(\omega_i t) + \sum_{i=N+1}^{2N} x_i \sin(\omega_{i-N} t)$$

$D_{Ph}^{a_k}$ can be defined as

$$D_{Ph}^{a_k}(\varepsilon(t)) = D^{a_k}(\varepsilon_{Ph}(t)) \tag{18}$$

where $\varepsilon_{Ph}(t)$ is given by the following equation:

$$\varepsilon_{Ph}(t) = \sum_{i=1}^{N} x_i \sin\left(\omega_i t + \frac{\pi b_k}{2}\right) + \sum_{i=N+1}^{2N} x_i \cos\left(\omega_{i-N} t + \frac{\pi b_k}{2}\right) \tag{19}$$

In the frequency domain the Fourier transform of $\varepsilon_{Ph}(t)$ and $G_{D_{Ph}^{a_k}}(t)$ can be related to the Fourier transform of $\varepsilon(t)$ by the following equations:

$$\varepsilon_{Ph}(\omega) = i^{b_k}\varepsilon(\omega) \tag{20}$$

$$G_{D_{Ph}^{a_k}}(\omega) = \omega^{a_k} i^{(a_k+b_k)}\varepsilon(\omega) \tag{21}$$

The phase-shifted fractional order derivatives of $\varepsilon(t)$ impart the anticlockwise hysteretic nature to the variation in $R(t)$ with $\varepsilon(t)$. The terms in

$$\sum_{l=1}^{N-M} C_{l+M} \int_0^t e^{-p_l(t-\tau)} \varepsilon(\tau)^{q_l} d\tau$$

are functions of strain, which keep increasing with time at a decaying rate for positive values of strain. These terms are used to take care of the property of the material, which causes its hysteresis loop to move upward with a number of cycles of applied strain.

By using the numerical scheme in Eq. (5) for fractional derivative and trapezoidal rule for integer order integral, the instantaneous value of resistance can be calculated at any time instant t_m by the following relation:

$$R(t_m) = R_1(t_m) + R_2(t_m) \tag{22}$$

where

$$R_1(t_m) = C_0\varepsilon(t_m) + \sum_{k=1}^{N} \frac{C_k \Delta t^{-a_k}}{\Gamma(2-a_k)} \left[\frac{(1-a_k)}{m^{(a_k)}} \varepsilon_{Ph}(t_0) + \sum_{j=0}^{m-1} ((j+1)^{(1-a_k)} - j^{(1-a_k)})(\varepsilon_{Ph}(t_{m-j}) - \varepsilon_{Ph}(t_{m-j-1})) \right]$$

and

$$R_2(t_m) = \sum_{l=1}^{N-M} \frac{C_{l+M}}{2} \left(e^{-p_l(t_m - t_0)}\varepsilon(t_0) + 2\sum_{j=0}^{m-1} e^{-p_l(t_m - t_j)}\varepsilon(t_j) + \varepsilon(t_m) \right) \Delta t$$

Here, $t_0 = 0$. $\varepsilon_{Ph}(\omega)$ can be calculated by using Eq. (19) after obtaining $\varepsilon(\omega)$ by performing fast Fourier transform (FFT) of $\varepsilon(t)$. Then by the inverse Fourier transform (IFFT) of $\varepsilon_{Ph}(\omega)$ and $\varepsilon_{Ph}(t)$ can be obtained. $\varepsilon_{Ph}(t)$ depends on unknown parameters b_k. Unknown parameters involved in Eq. (22) are $C_k(k=0,M)$, $a_k(k=1,N)$, $b_k(k=1,N)$, $p_k(k=1,M-N)$, and $q_k(k=1,M-N)$. These parameters have been found out by minimizing e in Eq. (16), where $R(t_m)$ is given by Eq. (22). The constraints used are $0 < a_k(k=1,N) < 1$ and $b_k(k=1,N) < 0$.

4.2 Model 2: Fractional Integral Model. In this model, the change in resistance has been taken as a combination of the changes in resistance caused by the instantaneous strain $\varepsilon(t)$ and its different fractional order integrals. So, the governing equation for this model is

$$R(t) = C_0\varepsilon(t) + \sum_{k=1}^{N} C_k J^{a_k}(\varepsilon(t)) \tag{23}$$

Using the numerical scheme described in Eq. (6), it can be written as

$$R(t_m) = C_0\varepsilon(t_m) + \sum_{k=1}^{N} \frac{C_k \Delta t^{a_k}}{\Gamma(2+a_k)} \left[\frac{(1+a_k)}{m^{(-a_k)}} \varepsilon(t_0) + \sum_{j=0}^{m-1} ((j+1)^{(1+a_k)} - j^{(1+a_k)})(\varepsilon(t_{m-j}) - \varepsilon(t_{m-j-1})) \right] \tag{24}$$

Hence, in submodel 1, the unknown parameters $C_k(k=0,N)$ and $a_k(k=1,N)$ were found out by minimizing the error defined in Eq. (16), after substituting $R(t_m)$ from Eq. (24). Constraints used in the minimization are $0 < a_k(k=1,N) < 1$.

Submodel 2 involves some modification of Eq. (23). In the frequency domain Eq. (23) can be defined as

$$R(\omega_j) = C_0\varepsilon(\omega_j) + \sum_{k=1}^{N} C_k (i\omega_j)^{-a_k} (\varepsilon(\omega_j)) \tag{25}$$

According to the discussion in Sec. 3, the multiplication of i^{-a_k} with each Fourier component of strain causes a phase-shift and imparts a hysteretic nature in the resistance-strain variation and multiplication of ω^{-a_k} with each Fourier component of strain causes the resistance-strain variation to be dependent on the rate of the application of strain. Submodel 2 aims to take care of these two effects independently. Hence, Eq. (23) was modified as

$$R(\omega_j) = C_0\varepsilon(\omega_j) + \sum_{k=1}^{N} C_k (i\omega_j)^{-a_k} i^{b_k} \varepsilon(\omega_j) \tag{26}$$

In time domain, Eq. (26) can be written as

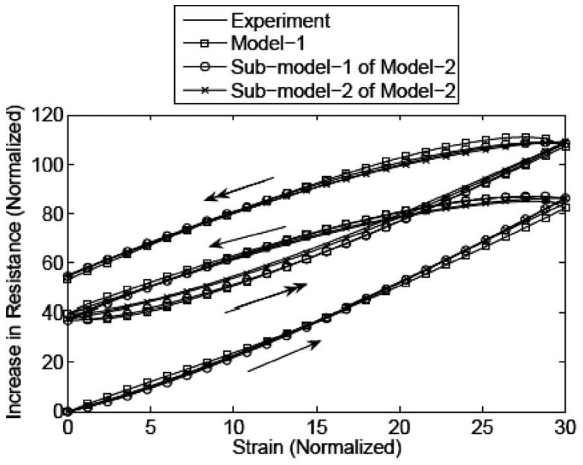

(a) Resistance vs. strain (dataset-1, N=3, M=6)

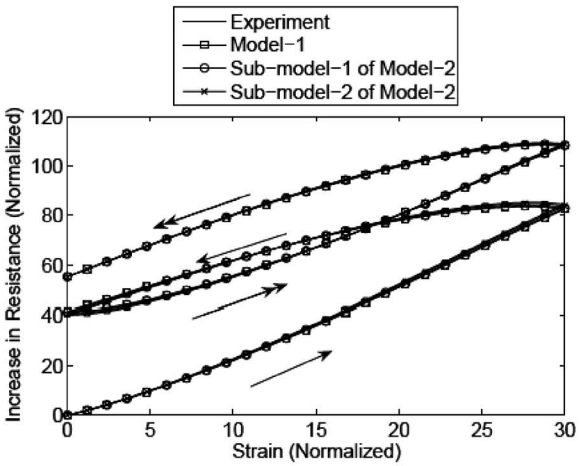

(b) Resistance vs. strain (dataset-1, N=5, M=8)

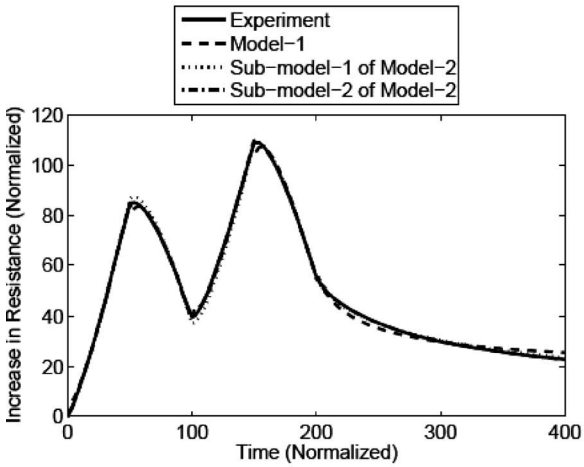

(c) Resistance vs. time (dataset-1, N=3, M=6)

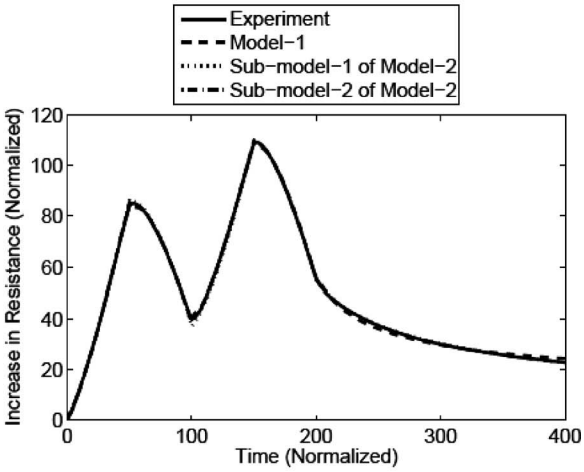

(d) Resistance vs. time (dataset-1, N=5, M=8)

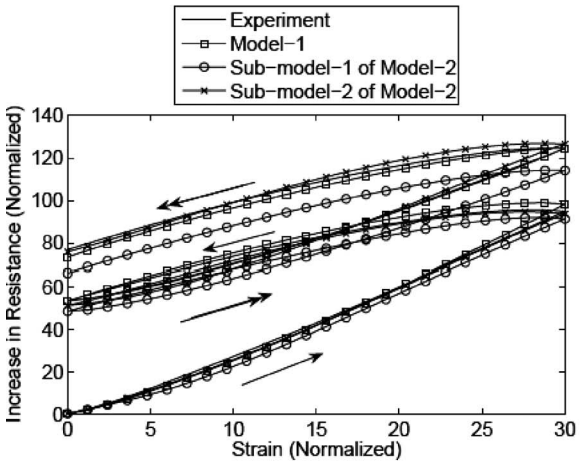

(e) Resistance vs. strain (dataset-2, N=3, M=6)

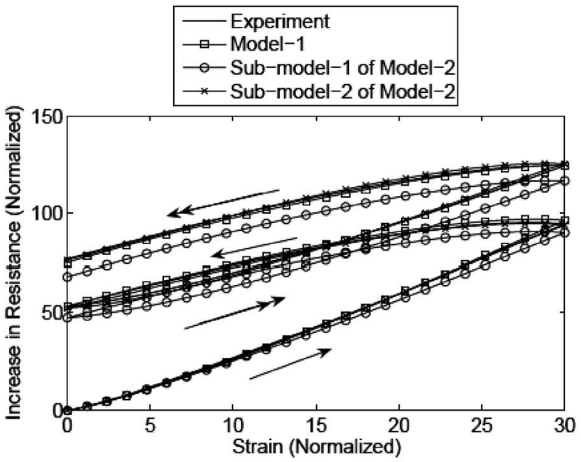

(f) Resistance vs. strain (dataset-2, N=5, M=8)

Fig. 6 Comparison of results from different models with experimental results

$$R(t) = C_0\varepsilon(t) + \sum_{k=1}^{N} C_k J_{\mathrm{Ph}}^{a_k}(\varepsilon(t)) \tag{27}$$

$$R(t_m) = C_0\varepsilon(t_m) + \sum_{k=1}^{N} \frac{C_k \Delta t^{a_k}}{\Gamma(2+a_k)} \left[\frac{(1+a_k)}{m^{(-a_k)}} \varepsilon_{\mathrm{Ph}}(t_0) + \sum_{j=0}^{m-1} \left((j+1)^{(1+a_k)} - j^{(1+a_k)} \right) \left(\varepsilon_{\mathrm{Ph}}(t_{m-j}) - \varepsilon_{\mathrm{Ph}}(t_{m-j-1}) \right) \right] \tag{28}$$

where $J_{\mathrm{Ph}}^{a_k}(\varepsilon(t)) = J^{a_k}(\varepsilon_{\mathrm{Ph}}(t))$, where $\varepsilon_{\mathrm{Ph}}(t)$ can be calculated following the procedure described in model 1.

The value of resistance at each data point can be calculated by the following equation:

Table 1 Values of parameters and errors in different models ($N=3$, $M=6$)

Model	Parameter	Value of the parameter	Errors (data set 1, data set 2) (%)
Model 1	$C_k(k=0,6)$	{−1000.0000, 662.5600, 419.5589, −221.7519, 1.6100, −1123.2110, 256.3312}	1.4539, 5.1200
	$a_k(k=1,3)$	{0.0501, 0.0499, 0.9800}	
	$b_k(k=1,3)$	{−0.1000, −0.1001, −1.9999}	
	$p_k(k=1,3)$	{0.0200, 10.000, 1.1211}	
	$q_k(k=1,3)$	{0.0001, 4.0001, 1.1000}	
Submodel 1 of model 2	$C_k(k=0,3)$	{−32.5047, 132.8861, 41.5930, 28.1075}	0.9970, 19.1000
	$a_k(k=1,3)$	{0.0001, 0.3930, 0.4102}	
Submodel 2 of model 2	$C_k(k=0,3)$	{21.9328, 9.3891, 15.4486, 100.4699}	0.7121, 4.1100
	$a_k(k=1,3)$	{0.6229, 0.5804, 0.3577}	
	$b_k(k=1,3)$	{0.9999, −0.9999, 0.1812}	

Table 2 Values of parameters and errors in different models ($N=5$, $M=8$)

Model	Parameter	Value of the parameter	Errors (data set 1, data set 2) (%)
Model 1	$C_k(k=0,8)$	{−756.9331, −301.9868, 590.4756, −258.7771, 624.0835, −78.0835, 146.7035, 2.1827, −1.6600}	1.0190, 3.0141
	$a_k(k=1,5)$	{0.0001, 0.0409, 0.9593, 0.0408, 0.0002}	
	$b_k(k=1,5)$	{−0.0002, −0.0801, −1.9999, −0.0901, −0.0005}	
	$p_k(k=1,3)$	{0.6269, 0.0176, 0.0177}	
	$q_k(k=1,3)$	{0.9716, 0.0045, 0.4755}	
Submodel 1 of model 2	$C_k(k=0,5)$	{5.0950, −61.3725, 253.7714, 97.4030, −46.0027, −66.1477}	0.7110, 17.0019
	$a_k(k=1,5)$	{0.3820, 0.1626, 0.9342, 0.4429, 0.9999}	
Submodel 2 of model 2	$C_k(k=0,5)$	{−136.1364, 61.8550, 44.8370, 132.1557, 139.4960, −84.1253}	0.6101, 3.0100
	$a_k(k=1,5)$	{0.0001, 0.5992, 0.5161, 0.0002, 0.5906}	
	$b_k(k=1,5)$	{0.0195, −0.7070, 0.1644, 0.0175, −0.1589}	

In this submodel $R(t_m)$ has been used and substituted in Eq. (16) from Eq. (28). By minimizing e with constraints $0<a_k(k=1,N)<1$ and $-1<b_k(k=1,N)<1$, unknown parameters $C_k(k=0,N)$, $a_k(k=1,N)$, and $b_k(k=1,N)$ have been determined.

5 Results From Error Minimization

Unknown parameters associated with different models have been estimated by minimizing the sum of the squares of errors e in the time interval (0,200) seconds (considering the cyclic variation in resistance with the cyclic strain only) of data set 1. Parameter estimation was done by assuming $N=3$ and $M=6$ and by assuming $N=5$ and $M=8$ to observe the improvement of results with an increase in the number of parameters. Using these parameters, the output resistance due to the type of input in data set 1 has been determined and its variation with strain and time has been shown from 0 s to 400 s in Figs. 6(*a*) and 6(*b*) and Figs. 6(*c*) and 6(*d*), respectively. Tables 1 and 2 show the unknown parameters obtained from error minimization. Using the parameters in Tables 1 and 2 a variation in electrical resistance for input in data set 2 was determined. Results are shown in Figs. 6(*e*) and 6(*f*). Tables 1 and 2 show the percentage of error in different models using various numbers of parameters. The error was calculated using the expression $((100\sqrt{\Sigma_{i=0}^{n}|R_{\mathrm{ex}}(t_i)-R(t_i)|})/(\Sigma_{i=1}^{n}|R_{\mathrm{ex}}(t_i)|))\%$.

6 Discussion

The comparison with experimental data set 1 shows that all the models are appropriate enough to simulate the path-dependent behavior of these materials for that strain rate. An increase in the number of terms involving both fractional derivative or fractional integral results in the improvement of the result. Results from all the models with $N=5$ and $M=8$ (for models 1 and 3) show quite a satisfactory match with the experimental result with very small errors. Parameters determined by minimizing the error in the time interval (0,200) seconds of data set 1 predicts the relaxation in the time interval (200,400) seconds accurately, as shown in Figs. 6(*c*) and 6(*d*). However, the model involving fractional integral (model 2) is more accurate as compared with the one involving fractional derivative (model 1). Including the effects of phase-shift and rate dependence independently (submodel 2 of model 2) imparts more flexibility to this model. But a comparison with experimental data set 2 obtained by applying time-dependent strain with a higher strain rate shows that submodel 1 of model 2 is not robust enough to take care of input rate dependence. Model 1 and submodel 2 of model 2 are more capable of taking care of the input rate dependence. Submodel 2 of model 2 matches the experimental results at different strain rates with minimum error.

7 Conclusion

Models based on fractional calculus have been developed to model the hysteresis in conductive polymers. The accuracy of the models have been explained by a comparison with the experimental result and their robustness has been verified by a comparison with the experimental results at different strain rates. Submodel 2 of model 2, involving linear function, fractional integral with phase-shifting was observed to be the most accurate and robust for our application. The proposed approach can be used to model any system with hysteresis.

Acknowledgment

The research was performed under Grant No. NNL05AA29G from the NASA Langley Research Center (NASA LaRC) and by the Institute for Critical Technologies and Sciences (ICTAS) at the

Virginia Polytechnic Institute and State University, Blacksburg, VA.

Nomenclature

- ε = strain
- R = resistance
- t = time
- ω = angular frequency
- γ = hysteresis operator in the Preisach model
- α = parameter, representing the up-switching value of the hysteresis operator in the Preisach model
- β = parameter, representing the down-switching value of the hysteresis operator in the Preisach model
- μ = weight function associated with γ in the Preisach model
- a = order of derivative and integral in the fractional calculus model
- b = parameter for phase-shifting in the fractional calculus model
- C = coefficients multiplied with strain and its different orders of derivatives and integrals in the fractional calculus model
- x = Fourier coefficients

References

[1] Hammerand, D. C., and Kapania, R. K., 1999, "Thermo-Viscoelastic Analysis of Composite Structures Using a Triangular Flat Shell Element," AIAA J., **37**(2), pp. 238–247.

[2] Hammerand, D. C., and Kapania, R. K., 2000, "Geometrically Nonlinear Shell Element for Hygrothermorheologically Simple Linear Viscoelastic Composites," AIAA J., **38**(12), pp. 2305–2319.

[3] Heymans, N., 2003, "Constitutive Equations for Polymer Viscoelasticity Derived From Hierarchical Models in Cases of Failure of Time-Temperature Superposition," Signal Process., **83**(11), pp. 2345–2357.

[4] Flandin, L., Brechet, Y., and Cavaille, J.-Y., 2001, "Electrically Conductive Polymer Nanocomposites as Deformation Sensors," Compos. Sci. Technol., **61**(6), pp. 895–901.

[5] Knite, M., Teteris, V., Kiploka, A., and Kaupuzs, J., 2004, "Polyisoprene-Carbon Black Nanocomposites as Tensile Strain and Pressure Sensor Materials," Sens. Actuators, A, **110**(1–3), pp. 142–149.

[6] Rekhviashvili, S. S., 2007, "Non-Steady-State Electrical Conduction of Polymers in the Model With Fractional Integro-Differentiation," Phys. Solid State, **49**(8), pp. 1598–1602.

[7] Viswamurthy, S. R., and Ganguli, R., 2007, "Modeling and Compensation of Piezoceramic Actuator Hysteresis for Helicopter Vibration Control," Sens. Actuators, A, **135**(2), pp. 801–810.

[8] Preisach, F., 1935, "Uber Die Magnetische Nachwirkung," Z. Phys., **94**, pp. 277–302.

[9] Everett, D. H., and Whitton, W. I., 1952, "A General Approach to Hysteresis," Trans. Faraday Soc., **48**, pp. 749–757.

[10] Cornejo, D. R., and Missell, F. P., 1999, "Application of the Preisach Model to Nanocrystalline Magnets," J. Magn. Magn. Mater., **203**, pp. 41–45.

[11] Roshko, R. M., and Huo, D. L., 2001, "A Preisach Characterization of the Barkhausen Spectrum of a Canonical Ferromagnet SrRuO3," Physica B, **306**(1–4), pp. 246–250.

[12] Vandenbossche, L., Dupré, L., and Melkebeek, J., 2005, "Preisach-Based Magnetic Evaluation of Fatigue Damage Progression," J. Magn. Magn. Mater., **290–291**(1), pp. 486–489.

[13] Schiffer, A., and Ivanyi, A., 2006, "Preisach Distribution Function Approximation With Wavelet Interpolation Technique," Physica B, **372**(1–2), pp. 101–105.

[14] Yu, Y., Xiao, Z., Lin, E.-B., and Naganathan, N., 2000, "Analytic and Experimental Studies of a Wavelet Identification of Preisach Model of Hysteresis," J. Magn. Magn. Mater., **208**(3), pp. 255–263.

[15] Oldham, K. B., and Spanier, J., 1974, *The Fractional Calculus*, Academic, New York.

[16] Chang, T., 2002, "Seismic Response of Structures With Added Viscoelastic Dampers," Ph.D. thesis, Virginia Polytechnic Institute and State University, Blacksburg, VA.

[17] Euler, L., 1738, "De Progressionibus Transcendentibus, Sev Quarum Termini Generales Algebraice Dari Nequent," Commentarii Academiae Scientiarum Imperialis Scientiarum Petropolitanae, **5**, pp. 38–57.

[18] Lacroix, S. L., 1819, *Traite du Calcul differentiel et du Calcul Integral*, 2nd ed., Courcier, Paris, pp. 409–410.

[19] Hardy, G. H., 1917, "On Some Properties of Integrals of Fractional Order," Messenger Math., **47**, pp. 145–150.

[20] Osler, T. J., 1970, "Leibniz Rule for Fractional Derivatives Generalized and an Application to Infinite Series," SIAM J. Appl. Math., **18**(3), pp. 658–674.

[21] Nutting, P. G., 1921, "A New General Law of Deformation," J. Franklin Inst., **191**, pp. 679–685.

[22] Bagley, R. L., and Torvik, P. J., 1983, "A Theoretical Basis for the Application of Fractional Calculus to Viscoelasticity," J. Rheol., **27**(3), pp. 201–210.

[23] Gemant, A., 1936, "A Method of Analyzing Experimental Results Obtained From Elasto-Viscous Bodies," Physica (Amsterdam), **7**, pp. 311–317.

[24] Scott-Blair, G. W., and Reiner, M., 1950, "The Rheological Law Underlying the Nutting Equation," Appl. Sci. Res., **A2**, pp. 225–234.

[25] Belavine, V. A., Nigmatullin, R. S., Miroshnikov, A. I., and Lutskaya, N. K., 1964, "Fractional Differentiation of Oscillographic Polarograms by Means of an Electrochemical Two-Terminal Network," Tr. Kazan. Aviacion. Inst., **5**, pp. 144–145.

[26] Bagley, R. L., and Torvik, P. J., 1983, "Fractional Calculus—A Different Approach to the Analysis of Viscoelastically Damped Structures," AIAA J., **21**(5), pp. 741–748.

[27] Bagley, R. L., and Torvik, P. J., 1986, "On the Fractional Calculus Model of Viscoelastic Behavior," J. Rheol., **30**(1), pp. 133–155.

[28] de Espindola, J. J., da Silva Neto, J. M., and Lopes, E. M. O., 2005, "A Generalised Fractional Derivative Approach to Viscoelastic Material Properties Measurement," Appl. Math. Comput., **164**(2), pp. 493–506.

[29] Horr, A. M., and Schmidt, L. C., 1996, "A Fractional-Spectral Method for Vibration of Damped Space Structures," Eng. Struct., **18**(12), pp. 947–956.

[30] Davis, G., Kohandel, M., Sivaloganathan, S., and Tenti, G., 2006, "The Constitutive Properties of the Brain Paraenchyma: Part 2. Fractional Derivative Approach," Med. Eng. Phys., **28**(5), pp. 455–459.

[31] Schmidt, A., and Gaul, L., 2006, "On the Numerical Evaluation of Fractional Derivatives in Multi-Degree-of-Freedom Systems," Signal Process., **86**(10), pp. 2592–2601.